

Two-phase flow in porous media: dynamical phase transition

Henning Arendt Knudsen^{1,2,*} and Alex Hansen^{2,†}

¹*Institute of Physics, University Duisburg-Essen, D-47048 Duisburg, Germany*

²*Department of Physics, Norwegian University of Science and Technology, NTNU, NO-7491 Trondheim, Norway*

(Dated: June 11, 2003)

Two-phase flow systems in porous media have complex dynamics. It is well established that a wide range of system parameters like viscosities and porosity as well as flow parameters such as pressure gradient and fluid saturation have strong impact on the dynamics. The transition from single-phase flow to two-phase flow is a dynamical phase transition. We discuss the order of the transition and investigate the phase diagram in parameter space, using a network simulator for two-phase flow. A semi-empirical theory for the location of the phase boundaries is provided.

PACS numbers: 47.55.Mh

I. INTRODUCTION

The field of two-phase flow in porous media is very rich on problems of a complex nature. These involve the study of properties on many different length scales and how to bridge the gap between the scales. Further, it is often possible to distinguish between the study of invasion processes and steady-state properties. The methods used in this field range from a set of experimental techniques, theoretical descriptions on different length scales to several numerical models or methods[1, 2].

In the petroleum engineering tradition, the main source of experimental information about flow systems has for decades been displacement experiments on core samples[3]. However, for increased theoretical or fundamental understanding, well controlled laboratory experiments have been the key. In particular, in the eighties, the experiments and simulations by Lenormand *et al.* lead to the development of a phase diagram for drainage, i.e., the displacement of a wetting phase by a nonwetting phase[4, 5]. Drainage was classified into the regimes stable displacement, viscous fingering, and capillary fingering. The regime boundaries depend on two dimensionless numbers, the capillary number Ca and the viscosity ratio M .

Two-phase flow consists of more than pure displacement processes. The complexity of ganglion dynamics and the existence of different regimes of flow of bubbles and blobs has been investigated experimentally by the Payatakes group[6, 7, 8]. They used etched glass networks for their studies, varying flow parameters within large ranges. By simultaneous injection of two fluids the experiments examine steady-state properties or close to steady-state properties.

We use a simulator for two-phase flow in porous media that is based on the Washburn equation[9], see Sec.II. This line of modeling dates back to the mid eighties to Koplik *et al.*[10]. The work by the Payatakes group is a

continuation of this tradition[11, 12]. Most of the work on two-phase flow simulation has been in the actual two-phase regime. That is to say that pure invasion processes like drainage were simulated until breakthrough of the nonwetting phase. The aforementioned regimes, the phase diagram, of drainage are well established and their properties much studied. When it comes to simulations for investigating steady-state properties, the majority of the work involves finding relative permeability curves for a wide range of parameters. Much effort has been put into making simulators that are specific for a given porous medium and fluid system. Further, other simulation techniques exist. On a even more detailed scale than our modeling is the work using lattice Boltzmann methods[13, 14, 15].

We wish here to take one step back and take a broader look at these systems. Assuming a porous medium with two phases, one wetting and one nonwetting with respect to the medium, there are three possible states of flow: only the nonwetting phase flows, only the wetting phase flows, or both flow simultaneously. Depending on a large set of parameters the system will find itself within one of these situations. Changing system parameters within appropriate ranges causes the system to undergo what is called a dynamical phase transition. Using the language of thermodynamics and critical phenomena we provide in this paper a phase diagram for steady-state flow. As was the case for the phase diagram of Lenormand *et al.* the capillary number and the viscosity ratio are the parameters of interest also in this primary study of the steady-state phase diagram.

We use a not too complex network simulator that can do real steady-state simulations. Nevertheless, the resulting phase diagram is complex. We believe that the structure of this diagram is of general interest. Phase boundaries are located by the simulations. Further, based on the simulations a semi-empirical theory for the location of the phase boundaries is given. We believe the overall structure of the phase diagram is universal for the two-phase flow system, whereas the exact positions of phase boundaries will vary from system to system.

*arendt@phys.ntnu.no

†alexh@phys.ntnu.no

II. MODEL

In order to investigate question of interest regarding two-phase flow in porous media it is possible to apply methods that count as theoretical, experimental or numerical. Experimental methods provide quantitative ‘correct’ results for the actual system investigated. However, results may differ from sample to sample or from system to system. By means of simulations the system properties can be controlled to a greater extent. This is highly advantageous when one wishes to study the effect of varying parameters of the system.

The results of the paper are based on a network simulator for immiscible two-phase flow. This line of modeling which is based on the Washburn equation[9] dates back to the work of several groups in the mid 1980’s[10, 11, 12]. Our model is a continuation of the model developed by Aker *et al.*[16, 17]. Although a thorough presentation can be found in [18], we provide for clarity a brief résumé of the main aspects.

The porous media are represented by networks of tubes, forming square lattices in two dimensions (2D) and cubic lattices in 3D, both tilted 45° with respect to the imposed pressure gradient and thus to the overall direction of flow. We refer to the the lattice sites where four(2D) and six(3D) tubes meet as nodes. Volume in the model is contained in the tubes and not in the nodes, although effective node volumes are used in the modeling of transport through the nodes. For further details, see[18]. Randomness is incorporated by distorting the nodes randomly within a circle (2D) and a sphere (3D) around their respective lattice positions. This gives a distribution of tube lengths in the system. Further, the radii are drawn from a flat distribution so that the radius of a given tube is $r \in (0.1l, 0.4l)$, where l is the length of that tube.

The model is filled with two fluid phases that flow within the system of tubes. The flow in each tube obeys the Washburn equation[9], $q = -(\sigma k/\mu)(\Delta p - \sum p_c)/l$. With respect to momentum transfer these tubes are cylindrical with cross-section area σ , length l , and radius r . The permeability is $k = r^2/8$ which is known for Hagen-Poiseuille flow[19]. Further, μ is the viscosity of the phase present in the tube. If both phases are present the volume average of their viscosities is used. The volumetric flow rate is denoted by q and the pressure difference between the ends of the tube by Δp . The summation is the sum over all capillary pressures p_c within the tube. With respect to capillary pressure the tubes are hour-glass shaped, meaning that a meniscus at position $x \in (0, l)$ in the tube has capillary pressure $p_c = (2\gamma/r)[1 - \cos(2\pi x/l)]$, where γ is the interfacial tension between the two phases. This is a modified version of the Young-Laplace law[1, 16].

Biperiodic (triperiodic in case of 3D) boundary conditions are used so that the flow is by construction steady flow. That is to say, the systems are closed so both phases retain their initial volume fractions, i.e., their sat-

urations. These boundary conditions are in 2D equivalent to a flow restrained to be on the surface of a torus. The flow is driven by a globally applied pressure gradient. Usually invasion processes are driven by setting up a pressure difference between two borders, inlet and outlet. Since, by construction, the outlet is directly joined with the inlet in our system, we give instead a so-called global pressure drop when passing a line or cut through the system[18, 20]. This is equivalent to imposing constraints on the pressure gradient that is experienced throughout the network. Integration of the pressure gradient along an arbitrary closed path one lap around the system, making sure to pass the ‘inlet-outlet’-cut once, should add up to the same global pressure difference.

The system is forward integrated in time using the Euler scheme. For each time step the distribution of the phases leads to a recalculation of the effective viscosities in the tubes and the capillary pressures across the menisci, and thus the coefficients in the equations for the pressure field. When the pressure field is known, the flow field follows automatically and the integration step may be performed. Details are found in[18].

III. PHASE DIAGRAMS

We present here phase diagrams for the dynamical properties of steady two-phase flow. The structure of the phase diagram is richer than one might naively believe. First we introduce the well-known concept of fractional flow (Eq.(2)) and provide a basic description of the nature of the two-phase flow system. We determine phase boundaries in the parameter space of saturation S_{nw} (defined in Eq.(1)), capillary number Ca (defined in Eq.(4)), and viscosity ratio M (defined in Eq.(3)). The definition of Ca is a crucial point since the definition is not unique. For the numerical exploration of the phase diagram one definition is used consistently in all simulation series: first at constant Ca and varying S_{nw} , second at constant S_{nw} and varying Ca . While Sec. III contains simulated diagrams, Sec. IV readdresses the definition of the capillary number and contains a semi-empirical theory for the location of the phase boundaries that are obtained in Sec. III. Upon presenting the method of finding the phase boundaries, the order of the transition is briefly discussed. However, the final discussion of the order is postponed to Sec. V.

A. Order parameter

In steady flow the volume fractions of the wetting and the nonwetting phase will not change in time. In our simulation model this requirement is fulfilled by having a closed system. The nonwetting saturation of the system is defined as

$$S_{nw} = \frac{V_{nw}}{V_{tot}}, \quad (1)$$

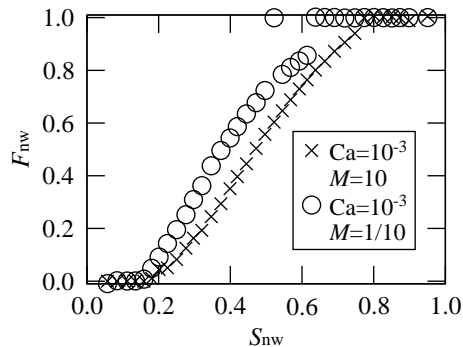


FIG. 1: The nonwetting fractional flow is shown as a function of nonwetting saturation for two sets of system parameters. Each data point is a result of simulation of the model system with the parameters in question until the system reaches steady state and the properties are measured. At low S_{nw} only the wetting phase flows and at high S_{nw} only the nonwetting phase flows. In-between there is a region of two-phase flow. We also observe that the transition of both curves from zero to nonzero F_{nw} is continuous. The transition of \times from two-phase flow to pure nonwetting flow is continuous or weakly first order, while the same transition for \circ is first order. There seems to be a clear jump in the value of F_{nw} as well as indications of hysteresis.

where V_{nw} and V_{tot} are the nonwetting and total volume, respectively. The wetting saturation S_w is defined similarly. For each value of the saturation one can in the simulations fix the total flux Q_{tot} in the system. In order to keep the total flux constant the imposed pressure gradient fluctuates in time around some typical mean value. This mean pressure is a function of saturation and total flux. Further, one can measure the flux of each of the phases in the system, Q_{nw} and Q_w , respectively. One defines the nonwetting fractional flow as

$$F_{nw} = \frac{Q_{nw}}{Q_{tot}}, \quad (2)$$

and likewise for the wetting fractional flow. A sample of nonwetting fractional flow as a function of nonwetting saturation is given in Fig. 1. The transport properties of the system depend on dimensionless groups of system parameters, namely the viscosity ratio and capillary number. We define the viscosity ratio as the nonwetting viscosity divided by the wetting viscosity;

$$M = \frac{\mu_{nw}}{\mu_w}. \quad (3)$$

Further, the capillary number is defined as

$$Ca = Ca_{dyn} = \frac{Q_{tot}\mu}{\gamma\Sigma}, \quad (4)$$

where γ is the interfacial tension between the two phases, Σ is the cross-section area of the system, and μ is the effective (weighted) viscosity of the system; $\mu = S_{nw}\mu_{nw} + S_w\mu_w$. Physically the capillary number measures the ratio between viscous and capillary forces in the

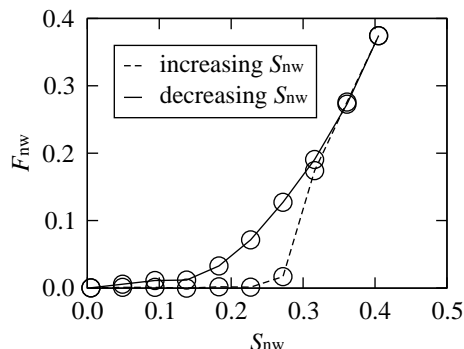
system. Using the weighted viscosity is motivated by the fact that when both phases flow, both viscosities play a role in determining the relative strength of viscous and capillary forces. We use this *dynamical* definition of Ca in this section, upon the exploration of the phase space. For convenience we leave out the subscript of Ca_{dyn} , but we will use it in the subsequent discussion in Sec. IV for clarity.

As illustrated in Fig. 1 fractional flow curves depend on M and Ca . This dependence is nontrivial. The curves exhibit three different regimes. For low nonwetting saturation only the wetting phase flows. Likewise, for high nonwetting saturation only the nonwetting phase flows. These two regions are thus effectively single-phase flow in a constraining environment consisting of both the solid porous medium and the immobilized phase. In-between these regions is the two-phase flow region. The crossovers from single-phase flow to two-phase flow are in fact dynamical phase transitions. We wish to study this system with that perspective. As order parameter for the transition from single wetting flow to two-phase flow we use the nonwetting fractional flow. Similarly we take the wetting fractional flow as the order parameter for the transition from single nonwetting flow to two-phase flow. In this way the order parameter is zero for single-phase flow and nonzero for two-phase flow.

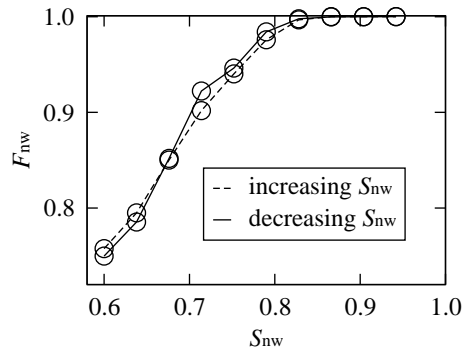
Having defined the order parameter, the nature of possible dynamical phase transitions in the system is well illustrated in Fig. 1. Starting at the left-hand-side, the transition is from single-phase wetting flow to two-phase flow when increasing the nonwetting saturation. Both samples show a continuous transition. That is to say that at least to the resolution of the curves the order parameter changes continuously from zero to nonzero values at the phase boundary. The transition of the curve marked with \circ on the right-hand-side has clear signs of being first order. Not only can we see how the order parameter is discontinuous, but the one isolated data point of $F_w = 0.0$ indicates the presence of hysteresis or history dependence in the system. Hysteresis is typical for first order transitions. In fact, we will use studies of hysteresis in order to unravel the nature of the phase diagram. As to the other curve, marked with \times , on the right-hand-side, the transition seems to be continuous or weakly first order.

B. Hysteresis loops

In order to map out the phase diagram, we need a tool that can locate the phase boundaries in parameter space. The order of the transitions should also be determined. Simulations of single points in parameter space to steady-state as in Fig. 1 are good for the part of parameter space where history effects are small. However, whenever one is close to a first order transition the history may give data points indicating single-phase flow or two-phase flow. It is possible to run simulations on sev-



(a) Single-phase wetting flow - two-phase flow



(b) Two-phase flow - single-phase nonwetting flow

FIG. 2: The stepwise simulation of two phase transitions. In both cases $Ca = 1.00 \times 10^{-3}$ and $M = 10$. The saturation is changed in steps up and down past the transition. The system is run for 7 seconds (physical time) at each step. (a) Starting at single-phase wetting flow, increasing the saturation above the transition to two-phase flow, and then lowering the saturation back to the initial level, the system shows hysteresis. (b) Starting in the two-phase region and increasing saturation to single-phase nonwetting flow, and decreasing again, no hysteresis appears.

eral statistically equal realizations of the porous media, as well as from various initial configurations, in order to find the region where both single-phase and two-phase flow are possible. The computations are somewhat computer demanding, and we have found it more efficient to simulate entire hysteresis loops to this effect. For instance starting at a specified saturation at which the system has two-phase flow, we change in a stepwise fashion the saturation slightly, run until steady-state, and measure the fractional flow. This is done until the system passes the transition to single-phase flow. Thereafter the saturation is changed the opposite way until the crossover from single-phase flow to two-phase flow occurs. In case of a continuous transition, these two points of transition will be the same. However, in case of a first order transition these points will not be the same, and the fractional flow will appear as a hysteresis loop, see Fig. 2(a).

It is also possible to keep the saturation constant and vary some other parameter, typically the capillary number. Similar loops are expected at first order transitions

by this procedure. The advantage of changing Ca is that one simply has to change the total flux Q_{tot} in the system. This is a unique operation, while changing the saturation smoothly is not unique. It requires that one makes a choice as to where in the system the changes should be made. In general, we increase or decrease existing bubbles by moving the menisci defining their surface. If the system is very fragmented, some smaller bubbles are typically also removed in order to reach the desired new saturation.

C. Diagrams for constant Ca

In this subsection we study one sample of the porous network of size 20×40 . We do not yet go into the possible dependence on size and topology, but focus on how the results depend on the three parameters: phase saturation, capillary number Ca , and viscosity ratio M . First we keep Ca and M constant while we vary the saturation stepwise over the transition from single-phase flow to two-phase flow and back.

Examples of transitions between single-phase and two-phase flow are shown in Fig. 2. By varying the saturation both ways over the transition, we observe how there can (a), and cannot (b), be hysteresis in the transition. Having a transition with little or without hysteresis as in Fig. 2(b), leads to a quite precise determination of the transition point. On the other hand it is not so clear where the transition occurs for the sample in Fig. 2(a). Not only are there two actual transition points, but these two points should be expected to depend on the actual path in parameter space. By that we mean in this case how many steps there are in saturation, and for what time the system is allowed to relax at each step. Further, the variation from sample to sample, or from realization to realization, of systems that are in principle similar, may very well be larger when there is hysteresis of this kind. For curves as in Fig. 2(b), the statistical variations are smaller. The transitions in Fig. 2 were taken to be at (a) $S_{nw} = 0.26$ and (b) $S_{nw} = 0.84$. Here we employed that convention that the system is single-phase whenever it is single-phase in one of the simulated directions. This definition is mainly motivated by the need of consistency in the extraction of data points in the following. This is in contrast to the more conventional definition, where the transition is located at the steepest point of the order parameter curve. However, this definition leads to too much noise in the analysis.

The range of capillary numbers studied is $Ca \in (3.16 \times 10^{-2}, 3.16 \times 10^{-4})$. On a base 10 logarithmic scale 9 values of Ca are chosen in steps of 0.25 from -1.50 to -3.50 . Similarly 21 values of M are chosen in steps of 0.25 in the interval $\log_{10} M \in (-2.50, 2.50)$, which means that $M \in (-3.16 \times 10^{-3}, 3.16 \times 10^2)$.

The resulting phase boundaries are shown in Fig. 3 as data points. The solid lines are constructed phase boundaries following from the semi-empirical theory given in

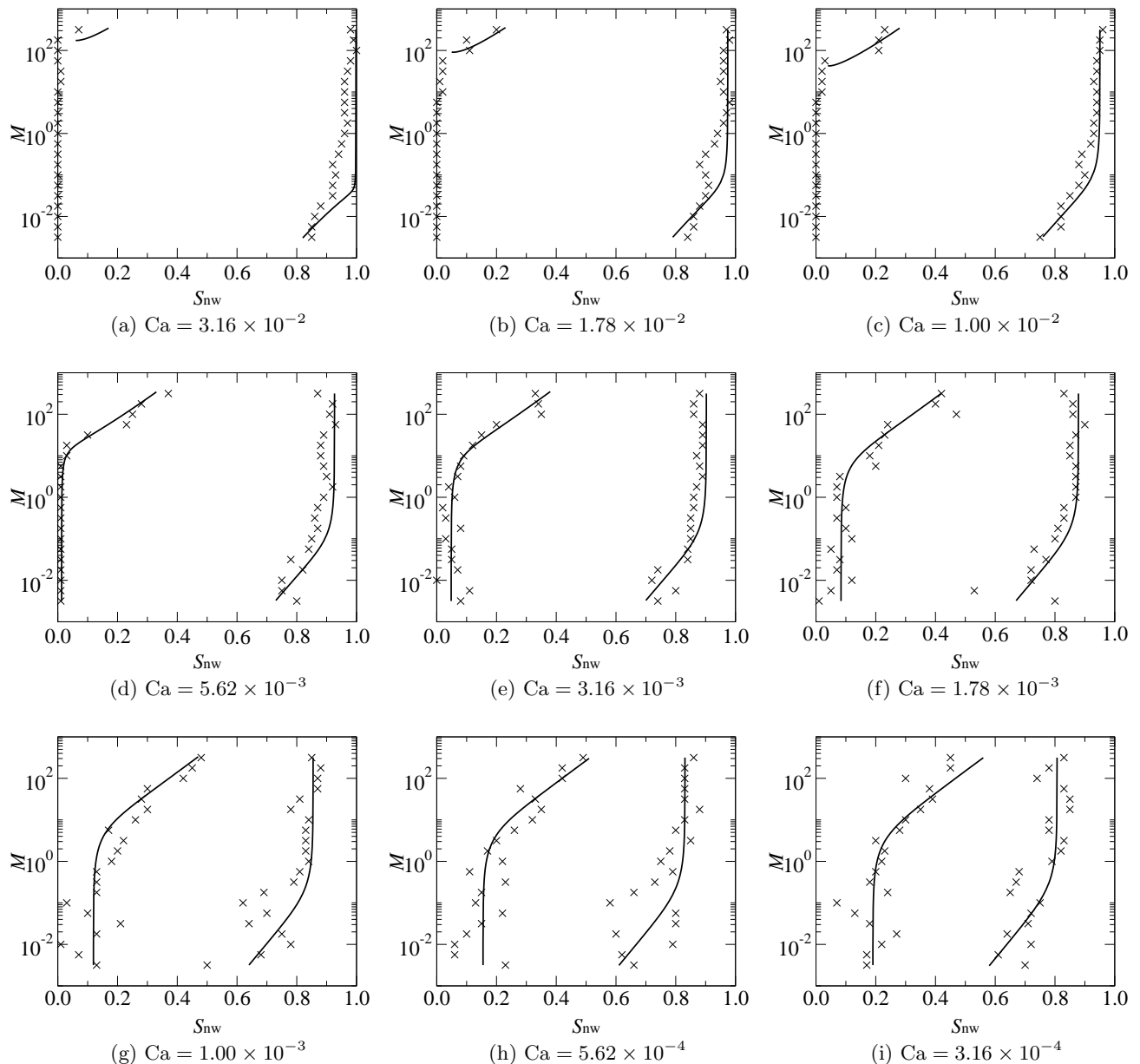


FIG. 3: The phase diagram for nine values of Ca . The \times -marks are the transition points from the simulations. The uncertainty in each point is not marked, but it is substantial. The scattering of points in parameter space gives an indication of the uncertainty. Phase boundaries are indicated by solid lines, see Sec. IV. The phase diagrams are divided into three regions, counting from the left-hand side: single-phase wetting flow, two-phase flow, and single-phase nonwetting flow.

Sec. IV. For now, let us consider the lines as visual aids to better see the phase boundaries in the diagrams. With increasing nonwetting saturation, the two lines separate the dynamical phases: single-phase wetting flow, two-phase flow, and single-phase nonwetting flow. Observe that for high capillary numbers the two-phase region spans almost all of the saturation range. As the capillary number is lowered, the single-phase regions grow in size. There is some kind of symmetry between the two transitions. That is to say the same effects occur on both sides, although not at the same numerical values.

In order to treat the two transitions simultaneously,

we employ the following notions. Since at each transition there is more volume of the phase that is close to single-phase flow, we refer to this phase as the majority phase. The other phase is the minority phase. On the left side the majority phase is wetting and the minority phase is nonwetting. Regarding viscosity ratios M there are basically three possibilities: viscosity matching phases, favorable viscosity ratio, and unfavorable viscosity ratio. Considering the system from the point of view of the majority phase, the viscosity ratio is favorable when the majority phase is the less viscous phase. Likewise, the viscosity ratio is unfavorable when the minority phase is

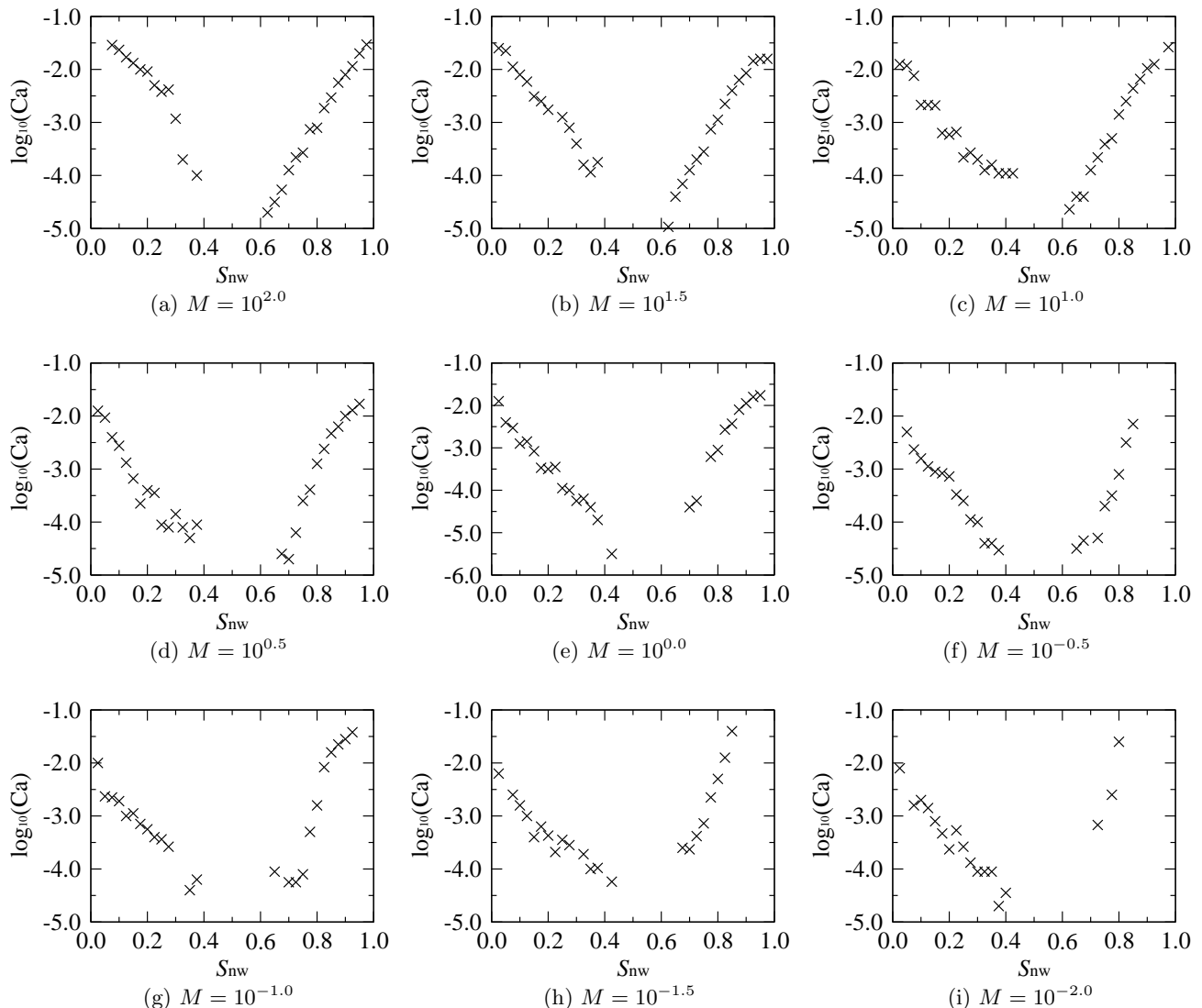


FIG. 4: The phase diagram for nine values of M . The simulations were performed at constant saturation, but with varying Ca. The simulated points indicate the dynamical phase boundaries. In the lower left part of the diagrams, there is single-phase wetting flow; in the middle upper part, two-phase flow; and in the lower right part, single-phase nonwetting flow.

less viscous. On the y -axes of Fig. 3 M varies over more than four decades. The positive side (on the logarithmic scale) is when the nonwetting phase is more viscous than the wetting phase. Thus, the viscosity ratio is favorable on the left side and unfavorable on the right side. For negative values of $\log_{10}(M)$ the ratio is unfavorable on the left side and favorable on the right side.

The general structure of the phase diagrams in Fig. 3 is as follows. First, consider the case of viscosity matching phases, $M = 1$. Here, we observe that for high capillary numbers the two-phase region spans almost all of the saturation range. As Ca is lowered the single-phase regions on each side open up, and the two-phase region becomes smaller. We cannot tell from the presented diagrams the limiting behavior of the phase boundaries for small Ca. However, since the nine diagrams in Fig. 3 are evenly distributed on the log-scale, one can conclude that, roughly

speaking, the dependence on Ca is logarithmic (also cfr. Fig. 4). It is reasonable to expect this behavior to persist also for lower Ca.

The dependence on M is interesting. For all values of Ca the fact that each curve has two main parts persists. Roughly, there is one situation for favorable viscosity ratios and another for unfavorable viscosity ratios. The subsequent discussion of these two situations are made from the two-phase flow point of view. The single-phase point of view is taken in Sec. IV.

For unfavorable viscosity ratio (lower left and upper right sides in each of the diagrams in Fig. 3) the phase boundaries are almost constant with respect to the value of M . As long as there are clear majority and minority phases, and one phase is close to going single-phase, the minority phase consists of bubbles and ganglions that are held back by capillary forces. It is always the case

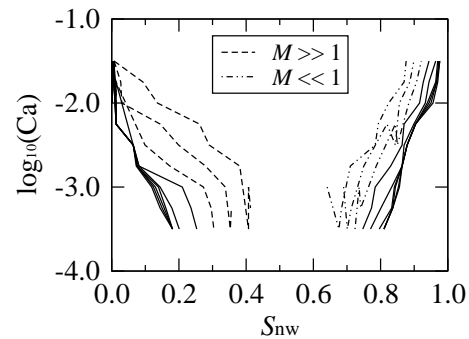
that the minority phase is held back in this way. However, when the viscosity ratio is unfavorable, the minority phase flows more easily. The viscous drag on the minority phase is thus negligible for this range of M -values explaining the constant location of the boundaries. This can be understood so that when the minority phase flows sufficiently easy, then it simply follows the majority phase around when capillary forces are overcome. Notice that the noise level increases with decreasing Ca . When the capillary forces become relatively stronger the motion of bubbles involves larger fluctuations, so this behavior is expected when properties are averaged over the same amount of time.

A different situation appears for favorable viscosity ratios. The capillary forces and viscous forces both try to hold back the minority phase. In this situation the actual viscosity ratio plays a role. The more favorable viscosity ratio, the more will the minority phase slow down. Because of the capillary forces the minority phase will not only slow down, but actually stop, and single-phase flow results. The border between two-phase flow and single-phase flow varies with M , as can be seen in Fig. 3. We observe the general trend that the single-phase region increases logarithmically with increasingly favorable viscosity ratio.

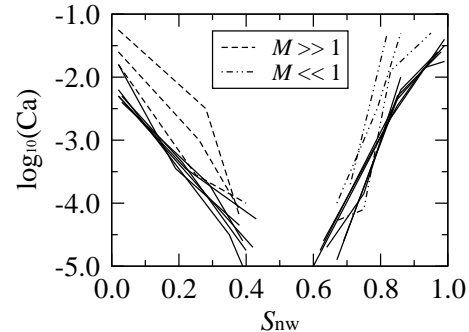
D. Diagrams for constant M

So far we have discussed the results from simulations where the saturation has been varied over the dynamical phase transition. In this subsection we present results from simulations in which the saturation and the viscosity ratio are held constant, while Ca is varied down and up again over the transition. Because of history effects and the fact that saturation and Ca are not varied in the same way, it is a priori not clear that the phase boundaries will be the same. Therefore, we check the results for consistency.

For nine different values of M , equidistantly distributed on a logarithmic scale between $M = 1/100$ to $M = 100$, simulations have been performed for a large set of saturations. The results are shown in Fig. 4. For large viscosity contrasts it turned out to be difficult to simulate very small saturations of the minority phase, possibly because the transition would occur for very large capillary numbers. More importantly, the central part of the saturation range was also difficult to simulate, because the fluctuations in the systems are larger in this region. One might expect that it is possible for the system to reach either single-phase wetting flow or single-phase nonwetting flow simply as the result of fluctuating into that state. We found that the fluctuations remain large for capillary numbers all the way down to $Ca = 10^{-6}$ for several samples. It is also possible that there is a finite saturation range, where the dynamical phase is two-phase flow for all values of Ca . We conclude that this region therefore may be out of reach. Even if we could get the results



(a) Extracted from Fig.3



(b) Extracted from Fig.4

FIG. 5: The phase boundaries from Figs. 3 and 4 are extracted as lines in a $S_{nw} - Ca$ coordinate system. Here, M parametrizes the curves and takes the same nine values as in Fig.4.

from the simulator, such low capillary numbers are outside the range where this simulator works well, and the relevance to physical systems would be limited.

The observations we can make from Fig. 4 are as follows. The nine presented diagrams have basically the same appearance. They consist of three parts: single-phase wetting flow in the lower left corner, single-phase nonwetting flow in the lower right corner, and two-phase flow in the upper middle region.

First, observe that as far as simulations have been performed, the phase boundaries have ending points at zero and unity saturation for finite values of Ca . At higher values of Ca the system has two-phase flow for all saturations. This is not surprising. High capillary numbers mean vanishing small capillary forces relative to viscous forces. In principle, as long as the viscosity contrast is finite or not too large, the more viscous phase would still flow unless there also are capillary forces to keep it from flowing. Hence, for these viscosity ratios, the capillary forces are too small above some threshold to prevent one phase from flowing.

Second, the general behavior of the two boundaries away from their end points, is that as Ca is lowered, the minority saturation increases. The meaning is simply that when the capillary forces become relatively stronger the single-phase regions grow in size. For low Ca values

the two-phase region becomes quite narrow. As we already have pointed out, we cannot tell whether the two boundaries meet in a triple point or if there will be a finite two-phase region also for smaller Ca .

In order to compare the curves in Fig. 4, the results have been extracted and put into one diagram, see Fig. 5(b). The curves overlap considerably so we have chosen to use the same line style for most of the lines. The exception is that for the three most favorable viscosity ratios of each transition a different line style is used. The three curves separate more and more from the rest of the curves with increasing viscosity contrast.

To compare the simulation results shown in Figs. 3 and 4, we exhibit data from Fig. 3 in Fig. 5(a). Here, the same set of viscosity ratios were used as in Fig. 5(b). This was done for best possible comparison. The line styles are also the same. Note that the range of capillary numbers in Fig. 5(a) is smaller than in Fig. 5(b). The results are not identical, but nevertheless quite close to each other within the overlapping range. We conclude that the two ways of performing the simulations give consistent results.

There are some general features of the diagrams in Fig. 5. First we observe that for both the left side boundary and the right side boundary, there seems to be a lower limit. This means that for all viscosity ratios, the respective single-phase region on each side extends at least to this limit. Roughly speaking these limits vary logarithmically with Ca . Again we cannot tell if this behavior will continue for lower Ca than depicted.

The other feature is that for higher Ca , say $Ca > 10^{-3.5}$, favorable viscosity ratio affects the phase boundary. To be precise, for the three intermediate values of M : $M = 10^{-0.5}$, $M = 1$, and $M = 10^{0.5}$, the phase boundaries on both sides are more or less equal to the limiting behavior just discussed. For these values of M , $M = 10^{1.0}$, $M = 10^{1.5}$, and $M = 10^{2.0}$, the viscosity ratio is favorable for the transition on the left side between single-phase wetting flow and two-phase flow. The corresponding three lines are marked with dashed lines. These values of M are unfavorable for the right-hand side transition. The last three values of M , $M = 10^{-1.0}$, $M = 10^{-1.5}$, and $M = 10^{-2.0}$, are favorable for the right-hand side transitions. They are indicated with dash-dotted lines. For the left-hand side these M values are unfavorable. In conclusion, there are six lines that are singled out for their favorable viscosity ratio. They clearly show how the single-phase regions become larger as the viscosity ratio becomes increasingly favorable. This effect can be seen in both Figs. 5(a) and 5(b).

IV. LOCATION OF THE PHASE BOUNDARIES

In the previous subsection the point of view taken was that of the two-phase flow system. That is to say, we used the dynamical definition of the capillary number,

Eq. (4), and we asked when does one of the phases cease to flow. Reversing the point of view is fruitful. Consider the system starting from a single-phase flow situation, the natural question is when does the second phase start to flow.

Being in a single-phase flow situation, although with both phases present in the system, means that the capillary number should be defined differently. Namely, the relevant viscosity is no longer the volume averaged viscosity, but the viscosity of the fluid that is actually flowing. The wetting and nonwetting capillary number is defined as

$$Ca_w = \frac{Q_{tot}\mu_w}{\Sigma\gamma}, \quad (5)$$

and

$$Ca_{nw} = \frac{Q_{tot}\mu_{nw}}{\Sigma\gamma}, \quad (6)$$

respectively. Here, Ca_w is the relevant capillary number for single-phase wetting flow, whereas, Ca_{nw} is relevant for single-phase nonwetting flow.

As opposed to the qualitative statements regarding the phase boundaries that were made in Sec. III, these definitions of the capillary number are also quantitatively useful. For a given system, i.e. given topology and saturation, the transition to two-phase flow takes place at a given wetting (or nonwetting) capillary number. That means with varying value of the viscosity ratio M , which also changes Ca_{dyn} , the relevant single-phase capillary number still holds a fixed value at the transition. This is plausible as long as the transition to two-phase flow is continuous. In that case the amount of minority phase flowing just after its mobilization is still only a small fraction of the total flow, and therefore the physical effective viscosity is still very close to the viscosity of the single-phase that just before flew alone. However, should the transition be first order so that a finite fraction is mobilized at once, then for large variations in M some corrections should be made. Nevertheless, for now we assume that the single-phase capillary number governs the location of the phase boundaries. The question of the order of the transition is addressed in Sec. V, and thereby the validity of this assumption is discussed.

We can write the dynamical capillary number

$$Ca_{dyn} = \frac{Q_{tot}\mu_w}{\Sigma\gamma} (S_w + MS_{nw}), \quad (7)$$

from which it follows that in the limit of small M

$$Ca_{dyn} = Ca_w S_w, \quad (8)$$

and in the limit of large M

$$Ca_{dyn} = Ca_{nw} S_{nw}. \quad (9)$$

In Fig. 5 we observe the limiting behavior for unfavorable M of the phase boundaries. There is on each side

a limiting line, below which there is always single-phase flow. By Eqs. (8) and (9) these limits are identified with the certain wetting or nonwetting capillary number for each value of the saturation determines the location of the transition. The limiting lines and the fitted functional relationships are shown in Fig. 6. We take this logarithmic dependency as an empirical input, and see which predictions can be made therefrom employing theory.

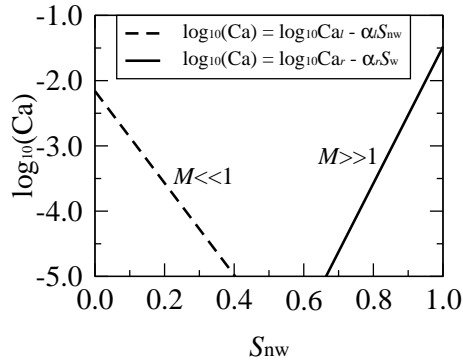


FIG. 6: The phase boundaries in Fig. 5 approach a limiting boundary for low M (left side) and large M (right side), and these limits are shown here. The fitted values for the constants are: $Ca_l = 10^{-2.16}$, $Ca_r = 10^{-1.48}$, $\alpha_l = 7.04$, and $\alpha_r = 10.42$.

We want to calculate the location of the phase boundaries for fixed dynamical capillary numbers as shown in Fig. 3. Considering first the left hand side (transition from wetting single-phase to two-phase flow), the criterion for the phase boundary is expressed as

$$Ca_w S_w = Ca_l 10^{-\alpha_l S_{nw}}, \quad (10)$$

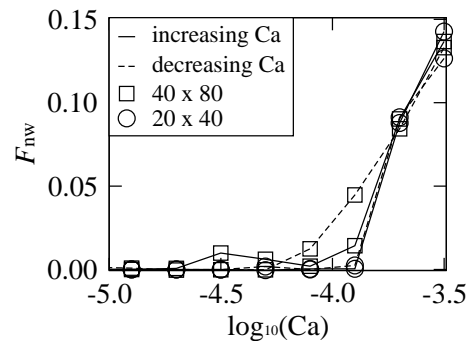
thus being a function of saturation. Letting Ca_{dyn} be fixed, this criterion inserted into Eq. (7) gives when solving for M as a function of S_{nw}

$$M = \frac{1 - S_{nw}}{S_{nw}} \left(\frac{Ca_{dyn} 10^{\alpha_l S_{nw}}}{Ca_l} - 1 \right). \quad (11)$$

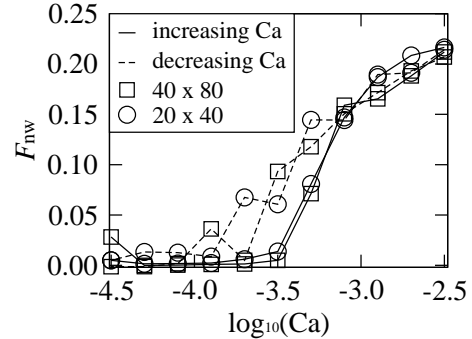
The interpretation of Eq. (11) is that for a fixed value of Ca_{dyn} the phase boundary is given by the set of values of M and S_{nw} that fulfill this relationship. For values of $Ca_{dyn} > Ca_l$, the wetting single-phase region does not exist, and so does the identification in the limit, Eq. (8) not apply. Still the criterion Eq. (10) can be used, and the result is that the single-phase region can only be reached for values of M larger than a certain threshold, see Fig. 3(a)-(c). This is not the case for $Ca_{dyn} < Ca_l$, where there is a single-phase region for all M .

In a similar way the boundaries on the right hand side between two-phase flow and single-phase nonwetting flow is found to obey

$$M = \left[\frac{1 - S_w}{S_w} \left(\frac{Ca_{dyn} 10^{\alpha_r S_w}}{Ca_r} - 1 \right) \right]^{-1}. \quad (12)$$



(a) $M = 1$



(b) $M = 10$

FIG. 7: Two samples of simulations on two different system sizes. The saturation is $S_{nw} = 0.3$ in both cases. The value of M is the only difference between (a) and (b). The transitions are (a) continuous or weakly first order, and (b) first order. The important aspect is that the hysteresis effects do not get smaller with increasing system size.

By using the Eqs. (11) and (12) the solid lines in Fig. 3 are the constructed phase boundaries for the respective values of Ca_{dyn} . The general good agreement between the simulated data points and these semi-empirical, semi-theoretical lines, serves as a confirmation a posteriori of this theoretical approach. Indeed, we conclude that the single-phase capillary number is the relevant entity that controls the transition to two-phase flow, rather than the more commonly used capillary number defined in Eq. (4). However, we should point out that from an experimental point of view, it is the conventionally defined capillary number which is the most relevant one.

V. ORDER OF THE TRANSITIONS

So far we have only discussed the location of the dynamical phase boundaries. The order of the transitions across these boundaries should also be discussed. All the simulations presented so far were done on a single system size, namely 20×40 nodes. It is necessary to take into account effects of changing the system size to determine the order of the transitions. However, first we present results for this system size.

Each simulation in Fig. 3 can be categorized into showing or not showing hysteresis. We look for the general trend while accepting that fluctuations and randomness play a role. Some realizations do not show hysteresis even though all neighboring points do, and vice versa. It turns out that the phase boundaries of Fig. 3 can be divided into two logical parts. The almost vertical line segments where the systems have unfavorable viscosity ratio differ from the other parts of the curves where the viscosity ratio is favorable. In the vertical parts the simulations show no or little signs of hysteresis in the order parameter. This indicates that the transitions in these regions are continuous. The fact that the curves are noisy for lower Ca in these regions, does not affect the order. In the sloping parts of the boundaries the order parameter exhibit discontinuity and hysteresis in most simulations. The level of hysteresis increase with increasing viscosity contrast. We claim that the transitions in these regions are first order.

Whether a transition is continuous or first order is a property connected to a specific path in parameter space. However, the paths in Fig. 3 and in Fig. 4 all mean a transition from single-phase flow to two-phase flow. We find similar hysteresis effect for both kinds of paths through parameter space.

In general, it is possible that the appearance of different orders of the transitions is a result of finite size effects. We have performed some selected simulations on a larger system size; 40×80 nodes. Comparisons between the results of the two system sizes are found in Fig. 7. The first order transition in (b) persist also for the larger system. If the signs of first order had been weaker for larger system sizes, then finite size effects had been the cause for apparent first order transitions. However, this is not the case here.

The noisy character of the vertical parts, showing continuous transitions, can be attributed to the geometrical heterogeneity of the system. Some parts of the system are more active in transportation than others. In such rather small systems self-averaging is small and by chance the minority phase is to a larger or smaller extent placed in inactive parts of the system. This gives a shift in position of the transition, i.e. noise, but does not affect the correlation between minority phase bubbles that are placed in active regions of the system. In fact these bubbles that are only held back by capillary forces are all correlated upon onset of mobilization. The motion of one bubble in one place relieves the pressure on all other minority bubbles in the system. The opposite is also true, when this bubble stops again, the pressure on the others increase immediately and this is likely to cause the onset of mobilization elsewhere. This is consistent with having infinite correlation length in statistical mechanics at continuous transitions.

The sloped sections of the boundaries, which from the hysteresis loop consideration show signs of first order transitions, show different characteristics. The viscosity ratio is unfavorable and the mobilization requires more

pressure on a bubble, but when mobilized, larger bubbles or connected bubbles are involved. However, this effect is more local in the sense that the minority phase is not moving a little bit here and a little bit there in the form of different bubbles, but rather one larger region moves for a longer time when it is first mobilized. This correspond to a non-infinite correlation length. Note that the system is driven by the global criterion of fixed total flux through the system. From this point of view, everything is all the time correlated with everything, so when we speak about correlations, we speak about the motions of the minority phase as they are observed.

VI. CONCLUSION

This study concerns steady-state properties of two-phase flow in porous media. Average flow properties are monitored by using a network simulator on pore level. A systematic change of the system parameters: phase saturation, viscosity ratio, and capillary number, is performed. We demonstrate how the system can be in either one of three dynamical states or phases. These are: single-phase wetting flow, two-phase flow, and single-phase nonwetting flow. Upon passing from one dynamical phase to another the system undergoes a dynamical phase transition. The phase diagram for the dynamical phases is revealed and its properties are discussed.

By means of hysteresis we determine the order of the phase transitions and we find that both continuous and first order transitions occur across different parts of the phase-boundaries. This is connected to two very different situations. One situation is when the viscosity ratio is defined to be favorable with respect to the majority phase: both capillary forces and viscous forces hold back the minority phase from flowing, next to this transition. The other case is when the viscosity ratio is defined to be unfavorable: only capillary forces try to hold back the minority phase next to the transition.

The phase diagram that is provided is for steady-state properties. This should be set in perspective to the phase diagrams by Lenormand *et al.* for drainage invasion flow properties[4, 5]. Although the fact that the system investigated is a particular steady-state two-phase flow system, we argue that the general structure of the dynamical phase diagram has a universally valid structure.

We find that the definition of the capillary number is of major importance. Whereas for the actual two-phase flow region we employ a volume averaged viscosity in the definition, it turns out that the actual locations of the phase boundaries are determined by the capillary number based on the viscosity of the single phase in question. Based on the relationships between the capillary numbers, theoretical part, and limiting of the phase boundaries, found by the simulations, we establish a semi-empirical theory for the location of the phase boundaries. Upon direct comparison this theory is found to be in agreement with the simulated data points.

Acknowledgments

H.A.K. thanks VISTA, a collaboration between Statoil and the Norwegian Academy of Science and Letters, for

financial support. We thank E. Skjetne for very valuable discussions, in particular in connection with Section IV where his contribution was substantial.

-
- [1] F. A. L. Dullien, *Porous Media: Fluid Transport and Pore Structure* (Academic Press, San Diego, 1992).
 - [2] M. Sahimi, *Flow and Transport in Porous Media and Fractured Rock* (VCH Verlagsgesellschaft mbH, Weinheim, 1995).
 - [3] D. Tiab and E. C. Donaldson, *Petrophysics* (Gulf Publishing Company, Houston, 1996).
 - [4] R. Lenormand, C. Zarcone, and A. Sarr, *J. Fluid Mech.* **135**, 337 (1983).
 - [5] R. Lenormand, E. Touboul, and C. Zarcone, *J. Fluid Mech.* **189**, 165 (1988).
 - [6] D. G. Avraam and A. C. Payatakes, *J. Fluid Mech.* **293**, 207 (1995).
 - [7] D. G. Avraam and A. C. Payatakes, *Transport in Porous Media* **20**, 135 (1995).
 - [8] D. G. Avraam and A. C. Payatakes, *Ind. Eng. Chem. Res.* **38**, 778 (1999).
 - [9] E. W. Washburn, *Phys. Rev.* **17**, 273 (1921).
 - [10] J. Koplik and T. J. Lasseeter, *Soc. Pet. Eng. J.* **25**, 89 (1985).
 - [11] G. N. Constantinides and A. C. Payatakes, *J. Colloid Interface Sci.* **141**, 486 (1991).
 - [12] G. N. Constantinides and A. C. Payatakes, *AIChE Journal* **42**, 369 (1996).
 - [13] D. H. Rothman, *J. Geophys. Res.* **95**, 8663 (1990).
 - [14] B. Ferreol and D. H. Rothman, *Transport in Porous Media* **20**, 3 (1995).
 - [15] K. Langaas and P. Papatzacos, *Transport in Porous Media* **45**, 241 (2001).
 - [16] E. Aker, K. J. Måløy, A. Hansen, and G. G. Batrouni, *Transport in Porous Media* **32**, 163 (1998).
 - [17] E. Aker, K. J. Måløy, and A. Hansen, *Phys. Rev. E* **58**, 2217 (1998).
 - [18] H. A. Knudsen, E. Aker, and A. Hansen, *Transport in Porous Media* **47**, 99 (2002).
 - [19] P. M. Gerhart, R. J. Gross, and J. I. Hochstein, *Fundamentals of fluid mechanics* (Addison Wesley, 1992), 2nd ed.
 - [20] S. Roux (unpublished).